Macromolecules **2003,** *36,* 3399−3410

Molecular Dynamics Simulations of Polyelectrolyte Solutions: Osmotic Coefficient and Counterion Condensation

Qi Liao,[†,‡] Andrey V. Dobrynin,[§] and Michael Rubinstein*,[†]

Department of Chemistry, University of North Carolina, Chapel Hill, North Carolina, 27599-3290; Polymer Physics and Chemistry Laboratory, Institute of Chemistry of the Chinese Academy of Sciences, Beijing 100080, P. R. China; and Polymer Program, Institute of Materials Science and Department of Physics, University of Connecticut, Storrs, Connecticut 06269-3136

Received December 20, 2002; Revised Manuscript Received March 3, 2003

ABSTRACT: Osmotic coefficients and counterion distribution functions of rodlike and flexible polyelectrolyte chains have been studied using molecular dynamics simulations of multichain systems with explicit counterions in salt-free solutions. Using the counterion density profile, we have verified different regimes in the phase diagram of rodlike and flexible chains predicted by the two-zone model of Deshkovski et al. The agreement between our simulation results and predictions of the two-zone model is reasonably good for weakly charged rodlike chains. However, for flexible chains our results for the distance dependence of the counterion density profile in different regions of the phase diagram are only in qualitative agreement with the predictions of the two-zone model. The osmotic coefficient changes nonmonotonically with polymer concentration, in agreement with predictions of the two-zone model. The osmotic coefficient decreases with increasing polymer concentration in dilute solutions of both rodlike and flexible polyelectrolytes. In semidilute solutions of flexible chains the osmotic coefficient is an increasing function of polymer concentration. We have found that position of the minimum in the osmotic coefficient is close to the overlap concentration.

1. Introduction

The osmotic pressure of polyelectrolytes in salt-free solutions exceeds the osmotic pressure of neutral polymers at similar polymer concentrations by several orders of magnitude.[1−9] It increases almost linearly with polymer concentration and is independent of the chain molecular weight in a wide range of polymer and salt concentrations.[1−9] This almost linear concentration dependence of the osmotic pressure is due to the contribution from counterions. However, experimentally measured osmotic pressure was found to be less than predicted by assuming that all counterions contribute to it.[2−9] This discrepancy can be qualitatively resolved by separating counterions into “free” and “condensed groups”.[10] Only free counterions are able to explore the solution volume V by each contributing of the order of k_BT/V to the osmotic pressure, where k_B is the Boltzmann constant and T is the absolute temperature. The condensed counterions are bound to the polyelectrolyte chain and do not contribute to the osmotic pressure. Thus, the osmotic pressure measurements allow a direct determination of the effective charge on the chain.

The two-state approximation for counterion distribution in a polyelectrolyte solution is an oversimplification of the real situation. A more rigorous description of the distribution of counterions and their contribution to the solution osmotic pressure can be obtained in the framework of the so-called cylindrical cell model.[11] Within the cell model the polyelectrolyte chains are arranged in a periodic array of parallel cylindrical cells. This model decouples the counterion and polymeric degrees of freedom, providing the equilibrium counterion density profile for the fixed idealized polymer conformation. The mean-field approximation of the counterion density profile is obtained by solving the nonlinear Poisson−Boltzmann equation describing the distribution of the electrostatic potential within the cylindrical cell. Unfortunately, the major limitation of the cylindrical cell model is that it is applicable only to semidilute polyelectrolyte solutions where the distance between chains is smaller than the chain size. According to this model, the osmotic coefficient ϕ, defined as the ratio of the solution osmotic pressure π to the ideal osmotic pressure k_BTc of all counterions

$$\varphi = \frac{\pi}{k_BTc} \tag{1}$$

has a weak concentration dependence and increases with polymer concentration. The cylindrical cell model qualitatively accounts for the concentration dependence of the osmotic coefficient in a variety of polyelectrolyte systems of flexible and rigid polyions.[2−5,9] The predictions of the cell model for counterion density profile and osmotic pressure were recently tested in molecular dynamics simulations of the cell model of rodlike chains.[12,13] These simulations demonstrate that even in the case of monovalent counterions the cell model underestimates the electrostatic interactions and overestimates the osmotic pressure. This disagreement is probably due to the correlation effects neglected by the mean-field model.

To avoid some of the limitations of the cell model and to describe the counterion distribution in dilute solutions, Deshkovski et al.[14,15] developed a two-zone model. In this model the volume occupied by charged rods is divided into two types of regions. The inner regions are

---

[†] University of North Carolina.

[‡] Institute of Chemistry of the Chinese Academy of Sciences.

[§] University of Connecticut.

* Corresponding author.

10.1021/ma0259968 CCC: $25.00

cylindrical zones around the charged rods with diameter of the order of the length of rod L. The outer regions are spherical zones outside the cylindrical regions that extend up to the distance between chains. It turns out that this model also has an exact solution of the nonlinear Poisson−Boltzmann equation for the electrostatic potential in the cylindrical regions around polyions.[14,15] In the limit when the outer (spherical) zone disappears, the solution of the two-zone model is reduced to that for the classical cell model.[11] The two-zone model predicts that in dilute solutions the osmotic coefficient decreases with polymer concentration whereas in semidilute solutions it increases with polymer concentration. Thus, the osmotic coefficient—and as a result, the fraction of free counterion—has nonmonotonic concentration dependence. However, the experimental data of the osmotic coefficient in solutions of rigid and flexible polyelectrolytes do not exhibit this nonmonotonic dependence on polymer concentration. Most experiments show that the osmotic coefficient remains virtually unchanged at low polymer concentrations and increases at higher polymer concentrations.[2−5,9,16,17] A possible explanation for the discrepancy between experimentally observed concentration dependence of the osmotic coefficient and the prediction of the two-zone model is that the polymer concentration is not low enough to show the upturn in the osmotic coefficient. However, a word of caution must be said: At very low polymer concentration the residual salt always dominates the osmotic pressure, leading to its quadratic decrease with decreasing polymer concentration (linear decrease of the osmotic coefficient). Thus, one has to take special precautions when preparing the sample to be able to experimentally observe the upturn in the osmotic coefficient.

The computer simulations of polyelectrolyte solutions are free from many complications arising in experiments—such as the presence of residual salt, chain polydispersity, and specific interactions of counterions—and are probably the easiest way to test the predictions of the two-zone model. The first detailed analysis of the osmotic pressure in molecular dynamics simulations of solutions of flexible polyelectrolytes was performed by Stevens and Kremer.[18] Their simulations confirmed that there are two different scaling regimes for osmotic pressure π. In a wide range of polymer concentrations covering both dilute and semidilute regimes the osmotic pressure, π, is controlled by counterions and varies almost linearly with polymer concentration, c. Strong deviation from the linear law occurs far above the chains' overlap concentration. In this high concentration regime the electrostatic interactions between charged monomers are almost completely screened, and the concentration dependence of the osmotic pressure crosses over to that for solutions of uncharged polymers. Stevens and Kremer[18] did not plot the dependence of the osmotic coefficient on polymer concentrations. The concentration dependence of the osmotic coefficient can be easily obtained by dividing the osmotic pressure data by concentration of counterions. Such analysis of their simulation data leads to a nonmonotonic dependence of the osmotic coefficient on polymer concentration (see Figure 10c in section 3). At low concentrations the osmotic coefficient decreases with increasing polymer concentration whereas at higher concentrations it increases with polymer concentration. There is a minimum of osmotic coefficient at the boundary between these two regimes. These results are in good agreement with the prediction of the two-zone model.[14,15]

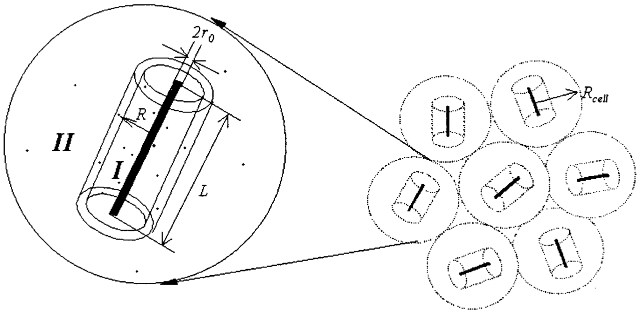

Figure 1. Schematic sketch of a dilute solution of rodlike polyelectrolytes and definition of different length scales for the two-zone model.

In the preceding paper,[19] we presented the results of the molecular dynamics simulations of structural properties of flexible polyelectrolytes in salt-free solutions. Our simulations confirmed the effect of counterions on chain conformations. Strongly charged polyelectrolytes reduce their effective charge by condensing counterions.[10] This counterion condensation leads to contraction of polyelectrolyte chains with increasing polymer concentration. In the present paper we relate the phenomenon of counterion condensation to the osmotic pressure and the osmotic coefficient of polyelectrolyte solutions. The results of molecular dynamics simulations of rodlike polyelectrolytes in a dilute solution are compared with the predictions of the two-zone model. To elucidate the effect of chain conformations (its internal degrees of freedom) on counterion condensation, we compare the results for rigid and flexible chains. The rest of the paper is organized as follows. In section 2 we briefly describe the results of the two-zone model.[14,15] The details of the molecular dynamics simulations are given in section 3. In sections 4 and 5 we analyze the phase diagrams, counterion distribution functions, the concentration dependence of the osmotic pressure, osmotic coefficient, and their relations with counterion condensation for rodlike and flexible polyelectrolytes. Finally, section 6 summarizes our results.

2. Two-Zone Model[14,15]

Consider a solution of cylindrical polyions with radius r_0, length L, and charge Q. A dilute solution can be modeled by placing each polyion at the center of a cell of size $R_{\text{cell}} \sim c_{\text{pol}}^{-1/3}$, where c_{pol} is the number density of polyions (see Figure 1). The cell volume is divided into two zones: a cylindrical zone (I), surrounding a rodlike polyion, and a spherical zone (II), outside the cylindrical region (see Figure 1). The electrostatic potential $\varphi(r)$ in the cylindrical zone I satisfies the Poisson−Boltzmann equation

$$\left(\frac{\partial^2}{\partial r^2} + \frac{1}{r}\frac{\partial}{\partial r}\right)\varphi(r) = \frac{4\pi e}{\epsilon}\, c(R)\, \exp\left(\frac{e\varphi(r)}{k_{\mathrm{B}}T}\right) \tag{2}$$

where r is the distance from the axis of the cylindrical polyion, e is the elementary charge, ϵ is the dielectric constant of the media, and $c(R)$ is the counterion concentration at the boundary of the cylindrical region where the electrostatic potential $\varphi(R)$ is set to zero.

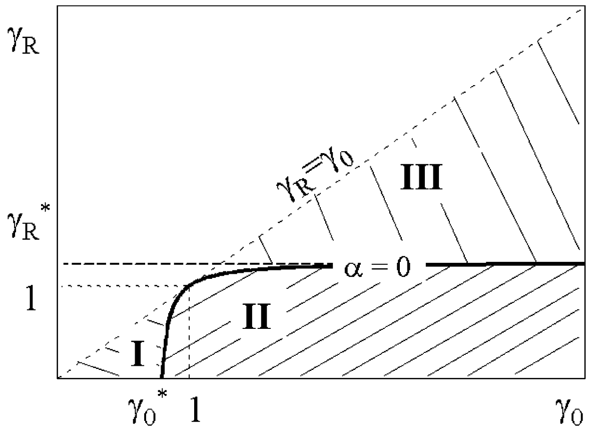

Figure 2. Theoretical phase diagram of the two-zone model. The parameter γ_0 is the bare linear charge density on polyion, and γ_R is the effective linear charge density of the cylindrical region. Phase I: weakly charged polyions. Phase II: saturated condensation. Phase III: unsaturated condensation. See text for details.

Here, we consider only systems with monovalent counterions. The inner boundary condition at the surface of the charged rod at $r = r_0$ is controlled by the reduced linear charge density $\gamma_0 = Ql_B/(eL)$

$$\left.\frac{\partial\varphi(r)}{\partial r}\right|_{r=r_0} = -\frac{2e}{\epsilon l_B}\frac{\gamma_0}{r_0} \tag{3}$$

where $l_B = e^2/(\epsilon k_B T)$ is the Bjerrum length. Note that the reduced linear charge density γ_0 is the dimensionless Manning counterion condensation parameter.[10] The outer boundary condition at $r = R$ is determined by the effective linear charge density of the cylindrical region $\gamma_R = Q_R l_B/(eL)$, where Q_R is the net charge within cylindrical region, which is equal and opposite to the charge of the outer region due to the electroneutrality condition.

$$\left.\frac{\partial\varphi(r)}{\partial r}\right|_{r=R} = -\frac{2e}{\epsilon l_B}\frac{\gamma_R}{R} \tag{4}$$

The solution of the nonlinear Poisson–Boltzmann equation (eq 2) with the boundary conditions (eqs 3 and 4) leads to the following counterion density profile in the cylindrical zone as a function of the distance r from the polyion axis[11]

$$c(r) = \frac{2}{\pi l_B}\frac{\alpha^2\zeta^{2\alpha}r^{2\alpha-2}}{[r^{2\alpha} - \zeta^{2\alpha}]^2} \tag{5}$$

where parameters α and ζ are defined by the following equations:

$$r_0{}^{2\alpha}\frac{\gamma_0 - 1 - \alpha}{\gamma_0 - 1 + \alpha} = \zeta^{2\alpha} = R^{2\alpha}\frac{\gamma_R - 1 - \alpha}{\gamma_R - 1 + \alpha} \tag{6}$$

Equation 6 represents the boundary conditions (eqs 3 and 4) in terms of the model parameters.

The exact solution of the two-zone model predicts three qualitatively different regimes shown in Figure 2 within the physical range $\gamma_0 > \gamma_R$ of linear charge densities γ_0 and γ_R. These regions are separated by the line $\alpha = 0$ (thick solid line in Figure 2)

$$\gamma_{0,\mathrm{crit}}(\gamma_R) = \frac{\gamma_R + (1 - \gamma_R)\ln(R/r_0)}{1 + (1 - \gamma_R)\ln(R/r_0)} \tag{7}$$

Phase I ($\gamma_R < \gamma_0 < \gamma_{0,\mathrm{crit}}(\gamma_R) < 1$) corresponds to real values of the parameter α (parameter α is proportional to $1 - \gamma_0$ for large R). In this regime the electrostatic attraction is not strong enough to keep counterions adjacent to the polyion, and most of the counterions are outside the cylindrical region. The counterion concentration in the cylindrical zone around the polyions has a power law dependence on the distance r from polyion $c(r) \propto r^{-2\gamma_0}$. Phase II corresponds to $\gamma_0 > \gamma_{0,\mathrm{crit}}$ and to the pure imaginary values of the parameter α. In this range of parameters the charge on the polyion is almost completely compensated by its counterions, and the counterion density profile is universal ($c(r) \propto r^{-2}$) and independent of the linear charge density γ_0 on the polyion. The line $\alpha = 0$ on this phase diagram (see eq 7) is the line of second-order phase transitions that separates phase II with the self-similar counterion density profile from phases I and III. Phase III corresponds to the condition $1 < \gamma_R < \gamma_0 < \gamma_{0,\mathrm{crit}}(\gamma_R)$ and to the real values of the parameter α (see Figure 2). Here, the counterion density profile is $c(r) \propto r^{-2\gamma_R}$.

To obtain an expression for the osmotic pressure in the framework of the two-zone model, one has to know the counterion concentration at the outer boundary of the spherical region. This requires knowledge of the electrostatic potential within the spherical zone. However, we can avoid solving the nonlinear Poisson–Boltzmann equation and use the relation between the pressure tensor $P(r)\delta_{\alpha\beta}$ and the Maxwell stress tensor $T_{\alpha\beta}(r) = (\epsilon/4\pi)(E_\alpha(r)E_\beta(r) + E^2(r)\delta_{\alpha\beta})$, where $\delta_{\alpha\beta}$ is the unit tensor and $E_\alpha(r)$ is the αth component of the electric field vector. Because the system is in equilibrium, the mechanical and electrostatic forces are balanced at each point within a cell. This leads to the following relation between the pressure and the Maxwell stress tensor

$$\nabla_\alpha P(r)\delta_{\alpha\beta} - \nabla_\alpha T_{\alpha\beta}(r) = 0 \tag{8}$$

The integral of the last equation over the volume of the spherical zone reduces to the integral over the zone boundaries. The value of the electric field at the outer boundary of the spherical zone is equal to zero due to electroneutrality of the two zones. The value of the pressure tensor at the outer boundary of the spherical region is equal to the osmotic pressure.

$$\pi = k_B T c(R) - \frac{\epsilon E^2(R)}{8\pi} = \frac{k_B T}{2\pi l_B R^2}((\gamma_R - 1)^2 - \alpha^2 - \gamma_R{}^2) \tag{9}$$

Dividing the osmotic pressure by the ideal pressure of all counterions, we obtain the prediction of the two-zone model for the osmotic coefficient

$$\varphi = \frac{V_{\mathrm{cell}}}{2V_{\mathrm{in}}\gamma_0}((\gamma_R - 1)^2 - \alpha^2 - \gamma_R{}^2) \tag{10}$$

where V_{cell} and V_{in} are the total cell volume and volume of the cylindrical region, respectively. Equation 10 for the osmotic coefficient reduces to that derived for the Katchalsky's cell model[15] in the case $\gamma_R = 0$ corresponding to semidilute solutions ($V_{\mathrm{cell}} = V_{\mathrm{in}}$)

$$\varphi_{\mathrm{cell}} = \frac{1 - \alpha^2}{2\gamma_0} \tag{11}$$

The osmotic coefficient in semidilute solutions (see eq 11) is proportional to the fraction of "free counterions" $1/\gamma_0$.[10,20,21]

Equation 10 can be simplified in the limit of not very large values of the parameter $\gamma_R \propto 1$ by assuming that the variations of the electrostatic potential over the spherical zone are small, and therefore, counterions are distributed almost uniformly in the spherical zone with the average concentration equal to that at the boundary of the cylindrical cell $c(R)$ (see ref 15)

$$c(R) = \frac{\gamma_R L}{l_B V_{\mathrm{out}}} = \frac{(\gamma_R - 1)^2 - \alpha^2}{2\pi l_B R^2} \tag{12}$$

where V_{out} is the volume of the outside (spherical) zone. Using this approximation, we can write the following expression for the osmotic coefficient of the two-zone model

$$\phi_{\mathrm{dilute}} \approx \frac{c(R)V}{Q} = \frac{\gamma_R}{\gamma_0}\left(1 + \frac{\pi L^3}{4V_{\mathrm{out}}}\right) \tag{13}$$

Equation 13 implies that at infinite dilution ($V_{\mathrm{out}} \to \infty$) the osmotic coefficient is proportional to the fraction of counterions that are outside the cylindrical zone γ_R/γ_0.

3. Model and Methodology

The solution of flexible polyelectrolytes is represented by an ensemble of M bead-spring chains of N monomers, N_c counterions per chain, and fraction of charged monomers $f = N_c/N$ confined in a cubic simulation box with periodic boundary conditions. All charged particles are taken to be monovalent ions, and therefore, the total number of charged monomers is equal to the number of counterions. Excluded-volume interactions between every pair of monomers and counterions are included via the truncated Lennard-Jones potential set to zero at the cutoff.[18,19] The connectivity of monomers in the chains is maintained by the finite extension nonlinear elastic (FENE) potential.[18,19] The solvent is modeled by a dielectric medium, with the dielectric constant ϵ such that all charged particles interact with each other via unscreened Coulomb potential $e^2/(\epsilon r) = k_B T l_B/r$. The value of the Bjerrum length l_B in all our simulations was set to 3σ, where σ is the parameter of the Lennard-Jones potential. The electrostatic interactions between all charges in the simulation box and all of their periodic images were computed by the smoothed particle mesh Ewald (SPME) algorithm.[22] We performed simulations of fully ($f = 1$) and partially ($f = 1/3$) charged flexible chains, with the chain degree of polymerization covering the interval N from 25 to 300. The model and simulation details for system of flexible polyelectrolytes have been described in the preceding paper.[19]

To compare counterion condensation in solutions of flexible and rodlike polyelectrolytes, we performed molecular dynamics simulations of the rodlike chains of overlapping spherical monomers with degree of polymerization $N = 97$. The bond length between monomers as well as their radius is equal to σ. Simulations were performed with $M = 16$ chains per simulation box with periodic boundary conditions. We performed simulations of charged rods with every monomer, every second monomer, every third monomer, and every sixth monomer charged, which allowed us to explore the range of linear charge densities $\gamma_0 = l_B/b = 3.0$, 1.5, 1.0, and 0.5, where b is the distance between charges along the chain contour. The simulations were performed at the monomer number density ranging from $10^{-7}\sigma^{-3}$ to $10^{-4}\sigma^{-3}$, corresponding to the dilute solution regime. The overlap concentration for the solution of rodlike polyelectrolytes with degree of polymerization $N = 97$, and size $L = 96\sigma$ is $c^* = 4N/\pi L^3 \approx 1.4 \times 10^{-4}\sigma^{-3}$.

Table 1. Phase Diagram of Rodlike Chains ($N = 97$)

	$f = 1/6$		$f = 1/3$		$f = 1/2$		$f = 1$	
c (σ^{-3})	γ_0	γ_R	γ_0	γ_R	γ_0	γ_R	γ_0	γ_R
1.0×10^{-4}	0.5	0.06	1.0	0.08	1.5	0.07	3.0	0.03
1.0×10^{-5}	0.5	0.30	1.0	0.71	1.5	0.76	3.0	0.90
1.0×10^{-6}	0.5	0.49	1.0	0.94	1.5	1.06	3.0	1.20

Since solvent in our simulations was modeled as a medium with effective dielectric constant, the pressure is equivalent to the osmotic pressure of a salt-free polyelectrolyte solution. In our simulations we measured the stress tensor $\mathbf{P}$.[23] The contribution of short-range interactions to the stress tensor $\mathbf{P}^{\mathrm{SR}}$ is

$$\mathbf{P}^{\mathrm{SR}} = -\frac{1}{V}\sum_{i<j}\langle \mathbf{r}_{ij} \otimes \mathbf{f}_{ij}^{\mathrm{SR}}\rangle \tag{14}$$

where $\otimes$ denotes the tensor product and $\mathbf{f}_{ij}^{\mathrm{SR}}$ is the force due to short-range interactions between ith and jth particle separated by distance $\mathbf{r}_{ij} = \mathbf{r}_i - \mathbf{r}_j$. The contribution of the electrostatic interactions $\mathbf{P}^{\mathrm{C}}$ to the stress tensor can be decomposed into the real space contribution, $\mathbf{P}^{\mathrm{dir}}$, the reciprocal space contribution, $\mathbf{P}^{\mathrm{rec}}$, and the correction component, $\mathbf{P}^{\mathrm{cor}}$ (see ref 22 for details). In the isotropic case the trace of the electrostatic contribution to the stress tensor Tr $\mathbf{P}^{\mathrm{C}}$ is equal to the negative of the electrostatic energy per unit volume. In the case of the rodlike chains (without intrachain interactions), we have corrected the expression for the osmotic pressure by eliminating the intrachain contributions.[22] In our simulations the osmotic pressure $\pi = \pi_{\mathrm{id}} - \mathrm{Tr}\,\mathbf{P}/3$ (where π_{id} is the ideal contribution to the osmotic pressure) was obtained by averaging the main diagonal components of the stress tensor $\mathbf{P}$ over the simulation run.

4. Tests of the Two-Zone Model

4.1. Rodlike Chains. a. Phase Diagram. We begin our test of the two-zone model by constructing the phase diagram for solutions of rodlike chains. The phase diagram for rodlike chains can be obtained either by changing the linear charge density γ_0 on the polyions or by changing their concentration. Both of these factors result in variations of the reduced linear charge density of the cylindrical region γ_R.

Table 1 summarizes our data for the phase diagram of rodlike chains shown in Figure 3. The thick solid line in Figure 3 is the analytical line $\alpha = 0$, separating different regimes in the phase diagram. The symbols represent the simulation results for the reduced linear charge density of the cylindrical zone γ_R for different values of the bare linear charge density γ_0 of the cylindrical polyion. In the case of rigid chains the parameter γ_R was obtained from integration of the counterion density $c(r)$. The counterion radial number density is defined as $c(r) = n(r)/v(r)$, where $n(r)$ is the number of

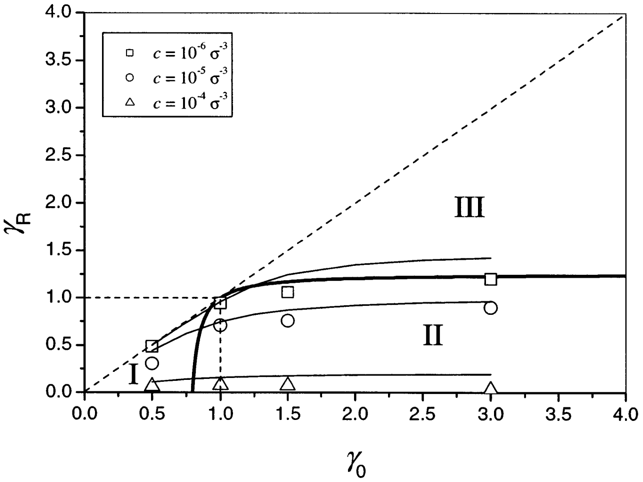

Figure 3. Phase diagram of rodlike polyions with $N = 97$. The thick solid line is the phase boundary, separating regime with counterion condensation ($\alpha = 0$). The thin solid lines are analytical solutions for effective linear charge density γ_R of the cylindrical region as a function γ_0 at different polymer concentrations $c = 10^{-6}$, 10^{-5}, and 10^{-4} (σ^{-3}), respectively (from top to bottom).

counterions in the cylindrical shell of radius and $v(r)$ is the shell volume. To minimize the end effects, only the counterions located in the interval $-L/4 < z < L/4$ from the center of the rod were taken into account in the evaluation of $n(r)$. The thin solid lines in Figure 3 are theoretical iso-concentration lines for the function $\gamma_R(\gamma_0)$. These lines are close to simulation points but consistently overestimate parameter γ_R in comparison with the simulation values by a small amount. This overestimation can be partially due to the correlations between charges ignored by the mean-field theory. The largest difference between simulation data and theoretical predictions is of the order of 0.2 and occurs for polymer concentrations close to the chains' overlap, where the two-zone model is the least applicable. Most of the simulation data corresponds to regime II with counterion condensation (see Figure 2).

b. Counterion Density Function. In Figure 4 we plot the counterion concentration around the rodlike polyions for the values of the parameter $\gamma_0 = 0.5$ (Figure 4a), 1.0 (Figure 4b), 1.5 (Figure 4c), and 3.0 (Figure 4d). The solid lines are analytical solutions (eq 5) of the nonlinear Poisson–Boltzmann eq 2 of the two-zone model. The agreement between simulation results and theoretical curves is very good in dilute solutions far from overlap concentration. However, as polymer concentration approaches the overlap concentration, the theoretical curves significantly overestimate the counterion density. We can also use these plots to verify the classification of the points into different regimes of the phase diagram (Figure 3). According to the prediction of the two-zone model, the counterion density profile $c(r)$ in region I of the phase diagram decays with distance r from the cylindrical polyion as $c(r) \propto r^{-2\gamma_0}$. Thus, the slope of this function depends only on the reduced linear charge density γ_0 on the rodlike polyion. This is exactly what we observe for the set of lines ($\gamma_0 = 0.5$) in Figure 4a. The slopes of the counterion density functions are close to $2\gamma_0$ (see Table 2). The largest deviation from the theoretical value does not exceed 6%. In the phase II region of the phase diagram the counterion density profile is universal $c(r) \propto r^{-2}$ and is independent of both parameters γ_0 and γ_R. The agreement between theoreti-

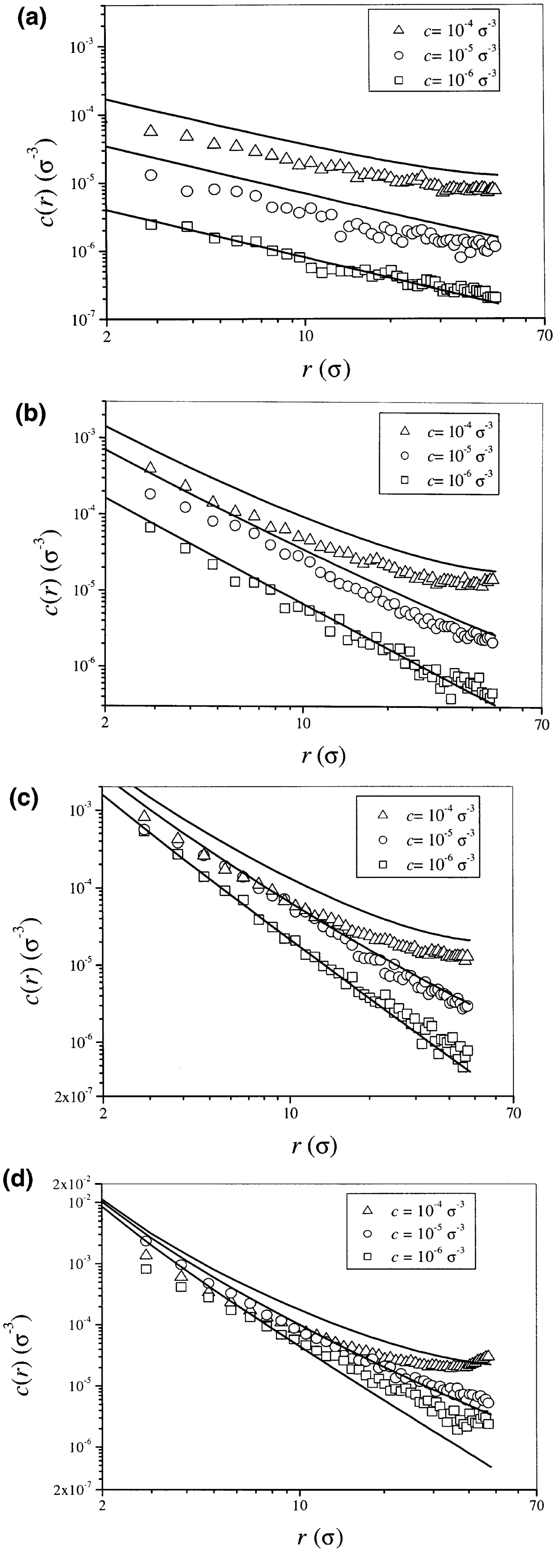

Figure 4. Counterion distributions around rodlike polyelectrolytes with bare linear charge densities $\gamma_0 = 0.5$ (a), 1.0 (b), 1.5 (c), and 3.0 (d). The solid lines are the analytical solutions of the nonlinear Poisson–Boltzmann equation of the two-zone model. The symbols are the simulation results for counterion distribution at different polymer concentrations $c = 10^{-4}$, 10^{-5} and 10^{-6} (σ^{-3}) in (a), (b), (c), and (d).

Table 2. Slopes of the Counterion Density Functions of Rodlike Chains Shown in Figures 8 Fitted in the Range $r = 2\sigma - 10\sigma$[a]

c (σ^{-3})	$\gamma_0 = 0.5$	$\gamma_0 = 1.0$	$\gamma_0 = 1.5$	$\gamma_0 = 3.0$
1.0×10^{-4}	−1.04 (−1)	−1.79 (−2)	−2.14 (−2)	
1.0×10^{-5}	−1.08 (−1)	−2.01 (−2)	−2.20 (−2)	−2.67 (−2)
5.0×10^{-6}				−2.75 (−2)
1.0×10^{-6}	−1.12 (−1)	−2.12 (−2)	−2.72 (−2.5)	

[a] Theoretical values are shown in parentheses.

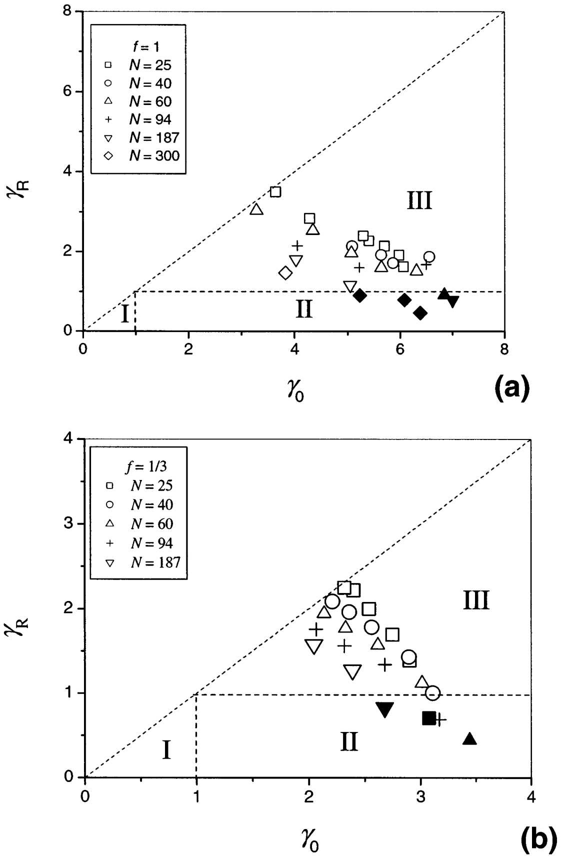

Figure 5. Phase diagrams for system of fully ($f = 1$) (a) and partially ($f = {}^1/_3$) (b) charged flexible polyions in dilute solutions. Open symbols represent points belonging to phase III, and filled symbols show the points within the counterion condensation region (phase II).

cal predictions and our simulation results is reasonable for all simulated concentrations with $\gamma_0 = 1$ and two polymer concentrations $c = 10^{-4}\sigma$ and $10^{-5}\sigma^{-3}$ for the reduced linear charge density $\gamma_0 = 1.5$ (see Table 2). However, the value of the slope −2.72 for the point with $c = 10^{-6}\sigma^{-3}$ and $\gamma_0 = 1.5$ is much larger than one would expect for the point within the phase II region. This point is very close to the boundary between phase II and phase III. In the phase III the counterion density profile is $c(r) \propto r^{-2\gamma_R}$. The slope −2.72 is closer to double the value of the reduced linear charge density γ_R of the cylindrical region $2\gamma_R = 2.5$. The agreement with predictions of the two-zone model is not so good for the larger value of the reduced linear charge density $\gamma_0 = 3$. Here, the counterion density decays much faster than predicted by the theory (see Table 2).

4.2. Flexible Chains. **a. Phase Diagram.** The extension of the two-zone model to flexible polyelectrolytes is not straightforward. The model was developed for solutions of charged cylinders with well-defined linear charge density γ_0 and well-defined radius r_0. It is therefore not directly applicable to flexible polyelectrolytes. The linear charge density is not well-defined for flexible polyelectrolytes because the backbone with charges is not straight. The backbone of flexible polyelectrolytes forms a complicated trajectory with shape changing with time and average shape changing with polymer concentration. The linear charge density of backbone charges depends on the distance between the point of observation and the nearest monomer. We define linear charge density γ_0 as the ratio of the net charge on the chain fN and the average value of the root-mean-square end-to-end vector R_e. Note that this linear charge density $\gamma_0 = fN/R_e$ is higher than the charge density “observed” from points within the “cylindrical” zone. Another parameter of the two-zone model that is not well-defined for flexible polymers is the cylinder radius r_0. We assume that the size r_0 of the effective cylinder is equal to σ. An important difference between rigid cylinders and flexible chains is that the latter shrink as polymer concentration increases, and therefore, the linear charge density of backbone charges γ_0 increases with polymer concentration.

The reduced linear charge density of the cylindrical region γ_R was obtained from integration of the counterion density function $c(r)$. To calculate $c(r)$, the space around flexible chain was divided into small cubes with volume Δv. The distance r is defined as the distance between the center of a cube and the closest monomer on the polymer backbone. During the simulation runs we calculated the average number $n(r)$ of counterions at distance r. The counterion density $c(r)$ is defined as $c(r) = n(r)/(m(r)\Delta v)$, where $m(r)$ is the number of cubes with volume Δv at distance r from the polymer backbone. Once again, to eliminate the end effects, only the counterions located in the interval $-R_e/4 < z < R_e/4$ from the center of mass of the chain along its elongation direction were taken into account.

Tables 3 and 4 summarize our data for the phase diagram of flexible chains. The classification of the points in Figure 5a,b was made by comparing γ_R with its critical value given by eq 7 for different chain lengths, polymer concentrations, and $r_0 = \sigma$. This choice of the diameter is not crucial because it enters eq 7 only logarithmically. The points in regime III are labeled as open symbols whereas the points in regime II are labeled as filled symbols. We can observe that in this case most of our simulation data correspond to regime III of the phase diagram.

b. Counterion Density Function. Figure 6 shows counterion density profiles around flexible chains for various chain lengths and charge parameters. For flexible chains, counterion distribution is controlled by the two factors. With increasing polymer concentration the fraction of counterions within the cylindrical region increases. This effect is similar to the solution of the rigid chains and is associated with the translational entropy of counterions. However, for flexible chains there is another effect: The increase of counterion concentration within the cylindrical region leads to contraction of polyelectrolyte chains.

We performed the same analysis of the counterion density function $c(r)$ in the solutions of flexible chains as in the case of rodlike chains. The agreement between predictions of the two-zone model for the slope of the counterion density function $c(r)$ and our simulation results for the systems of flexible chains is not as good

Table 3. Phase Diagram of Fully Charged Flexible Chains ($f = 1$)

	$N = 25$		$N = 40$		$N = 60$		$N = 94$		$N = 187$		$N = 300$	
C (σ^{-3})	γ_0	γ_R	γ_0	γ_R	γ_0	γ_R	γ_0	γ_R	γ_0	γ_R	γ_0	γ_R
3.0×10^{-3}	6.06	1.62										
1.5×10^{-3}	5.98	1.91	6.56	1.87	6.84	0.91						
5.0×10^{-4}	5.70	2.14	5.87	1.72	6.32	1.52						
1.5×10^{-4}	5.41	2.27	5.64	1.92	5.64	1.60	6.50	1.68	7.00	0.79		
1.0×10^{-4}											6.38	0.47
5.0×10^{-5}	5.30	2.39									6.08	0.79
1.5×10^{-5}			5.08	2.14	5.07	1.97	5.22	1.61	5.05	1.16	5.23	0.91
1.5×10^{-6}	4.39	2.84			4.35	2.53	4.06	2.15	4.03	1.81	3.83	1.47
1.5×10^{-7}	3.65	3.50			3.28	3.03						

Table 4. Phase Diagram of Partially Charged Flexible Chains ($f = {}^1/_3$)

	$N = 25$		$N = 40$		$N = 60$		$N = 94$		$N = 187$	
c (σ^{-3})	γ_0	γ_R	γ_0	γ_R	γ_0	γ_R	γ_0	γ_R	γ_0	γ_R
1.5×10^{-2}	3.08	0.705								
5.0×10^{-3}	2.90	1.39	3.11	1.00	3.44	0.44				
1.5×10^{-3}	2.75	1.69	2.90	1.43	3.01	1.12	3.17	0.69		
1.5×10^{-4}	2.54	2.00	2.56	1.78	2.61	1.57	2.68	1.34	2.68	0.83
1.5×10^{-5}			2.36	1.96	2.32	1.77	2.31	1.56	2.39	1.27
1.5×10^{-6}	2.40	2.22	2.21	2.09	2.14	1.94	2.06	1.76	2.05	1.58
1.5×10^{-7}	2.32	2.25								

Table 5. Slopes of the Counterion Density Functions of Flexible Chains Shown in Figures 9 Fitted in the Range $r = 1\sigma$–5σ[a]

c (σ^{-3})	(a) $N = 94$, $f = {}^1/_3$	(b) $N = 187$, $f = {}^1/_3$	(c) $N = 94$, $f = 1$	(d) $N = 187$, $f = 1$
1.5×10^{-3}	−2.41 (−2)			
1.5×10^{-4}	−2.24 (−2.68)	−2.30 (−2)	−2.40 (−3.26)	−2.34 (−2)
1.5×10^{-5}	−2.46 (−3.12)	−2.39 (−2.54)	−2.73 (−3.22)	−2.84 (−2.32)
1.5×10^{-6}	−2.62 (−3.52)	−2.45 (−3.16)	−3.59 (−4.3)	−3.42 (−3.62)

[a] Theoretical values are shown in parentheses.

as for the systems of rodlike chains. For flexible chains the difference between simulation results and theoretical values is within 40% (see Table 5). But the two-zone model is not expected to work quantitatively well for flexible polyelectrolytes.

5. Osmotic Coefficient of Polyelectrolyte Solutions

5.1. Dilute Solutions. Figure 7 shows the osmotic coefficient of rodlike (Figure 7a) and flexible fully charged (Figure 7b) polyelectrolytes in a dilute salt-free solution. The solid lines in Figure 7a are predictions of a two-zone model (eq 13). These figures show a decrease in the osmotic coefficient ϕ with increasing of polymer concentration c. This behavior is not only in good qualitative agreement, but for some data, even in good quantitative agreement with the predictions of the two-zone model. To verify the predictions of eq 13 for the osmotic coefficient, Figure 8 shows a universal plot of reduced osmotic coefficient in $\gamma_0\ \phi/\gamma_R$ as a function of normalized polymer concentration c/c^*. For the rodlike chains we defined the overlap concentration c^* to be equal to $4N/(\pi L^3)$. All points collapse onto the universal curve as predicted by eq 13 for rodlike polyelectrolyte solutions (see Figure 8a). However, the size R_e of flexible chains is a function of polymer concentration—polyelectrolytes contract with increasing concentration. To collapse all points into one universal curve and to take into account the chain contraction in Figure 8b, we plotted reduced osmotic coefficient $\gamma_0\ \phi/\gamma_R$ vs the ratio of polymer concentration c to monomer concentration within cylindrical region $c\pi[R_e(c)]^3/(4N)$. All points once again collapse into one universal curve, proving that the two-zone model adequately describes our simulation results for flexible chains as well. A reasonable collapse of our data can also be obtained by plotting $\gamma_0\ \phi/\gamma_R$ vs c/c^* (see Figure 8c). However, in this case the collapse is not as good as in Figure 8b. The success of eq 13 in describing our simulation results can be used to experimentally estimate the fraction of counterions γ_R/γ_0 distributed outside the volume of a polyelectrolyte chain. According to eq 13, this fraction can be estimated as

$$\frac{\gamma_R}{\gamma_0} \approx (1 - c/c^*)\varphi \qquad (15)$$

5.2. Semidilute Solutions. In Figure 9 we plot concentration dependence of the osmotic coefficients of fully (Figure 9a) $f = 1$ and partially (Figure 9b) $f = {}^1/_3$ charged flexible chains in a Θ-solvent. To compare our results with previous computer simulations by Stevens and Kremer,[18] their data are shown in Figure 9c. The positions of overlap concentrations are marked by arrows. We can observe that the osmotic coefficient has nonmonotonic dependence on polymer concentration. It decreases with polymer concentration in dilute solutions and increases with the polyelectrolyte concentration above the overlap concentration. Far above the overlap concentration, the osmotic coefficient is almost independent of the chain degree of polymerization N, and all points collapse onto one curve. At higher polymer concentrations both our simulation results and the results presented in ref 18 suggest that the concentration dependence of the osmotic pressure approaches that of uncharged polymers in good solvents.

According to the scaling theory, the osmotic pressure of semidilute polyelectrolyte solutions is the sum of polymer and counterion contributions[24,25]

$$\frac{\pi}{k_B T} = cf_e + \frac{1}{\xi^3} \qquad (16)$$

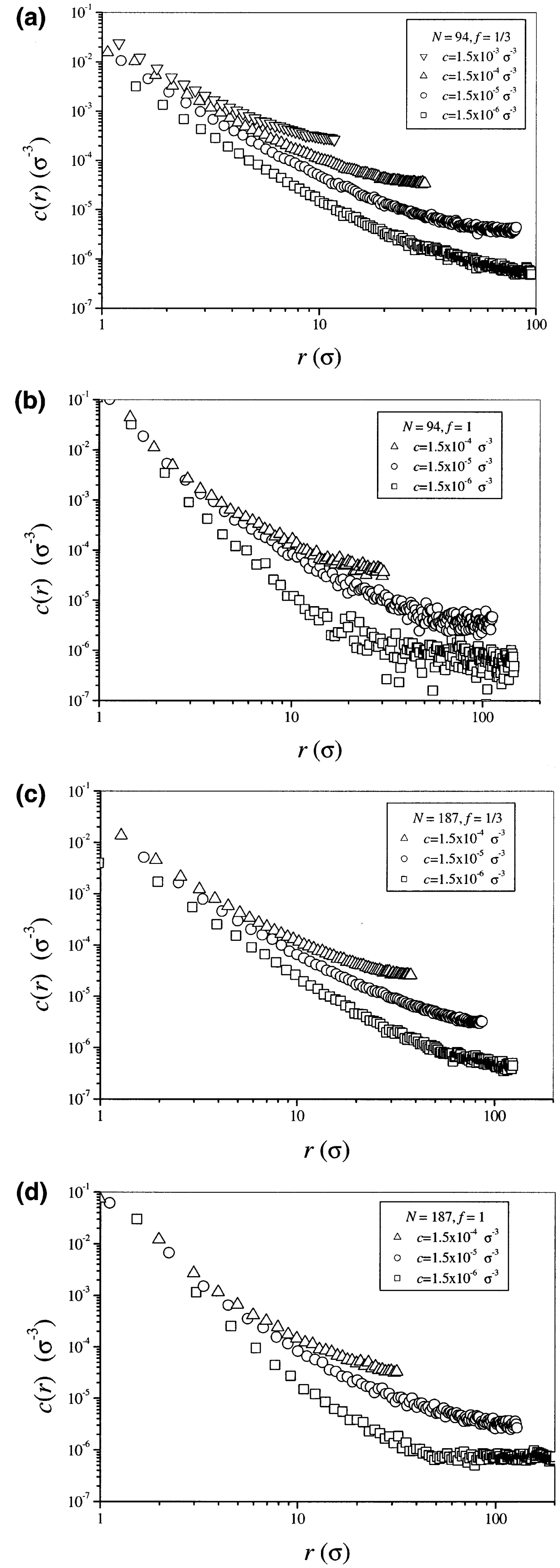

Figure 6. Counterion distribution around flexible polyions as a function of shortest distance r to the monomer on a chain. (a) $N = 94$, $f = {}^1/_3$; (b) $N = 94$, $f = 1$; (c) $N = 187$, $f = {}^1/_3$; (d) $N = 187$, $f = 1$.

where f_e is the fraction of effective charges and ξ is the correlation length of semidilute polyelectrolyte solutions.

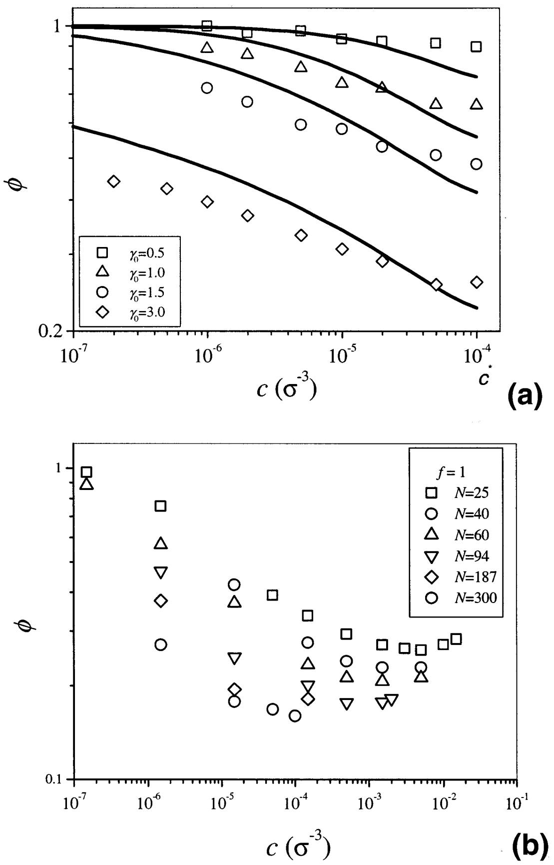

Figure 7. (a) Dependence of osmotic coefficient of rodlike polyions on polymer concentration in dilute solutions. Open symbols are simulation results. The lines are predictions of zero-order approximation of the two-zone model. From top to bottom, the parameter γ_0 is 0.5, 1.0, 1.5, and 3.0, respectively. (b) Dependence of osmotic coefficient of flexible polyions on polymer concentration in a dilute solution of strongly charged polyelectrolyte chains ($f = 1$).

In semidilute polyelectrolyte solutions the correlation length ξ is inversely proportional to the square root of polymer concentration, $\xi \sim c^{-1/2}$, whereas in solutions of neutral polymers in good solvent conditions it has stronger concentration dependence $\xi \sim c^{-3/4}$ (see ref 26). Dividing the osmotic pressure eq 16 by counterion concentration, one finds the expression for the osmotic coefficient in a semidilute polyelectrolyte solution

$$\varphi = f_c + \frac{1}{c\xi^3} \tag{17}$$

To evaluate the importance of the two terms in eq 17, we present in Figure 10 the total osmotic pressure π of a semidilute polyelectrolyte solution of fully charged chains with $N = 300$ (squares), together with polymeric contribution to the osmotic pressure (circles). The polymeric contribution is estimated as k_BT/ξ^3. The correlation length ξ was evaluated from the intra- and interchain correlation functions by the method described in our previous publication.[19] As one can see, the polymeric contribution to the osmotic pressure is negligible at lower concentrations. It becomes of the same order of magnitude as the total osmotic pressure at polymer concentrations of the order of 100c*. Thus, the osmotic pressure of semidilute polyelectrolyte solutions is dominated by pure counterion contribution over a wide range of polymer concentrations.

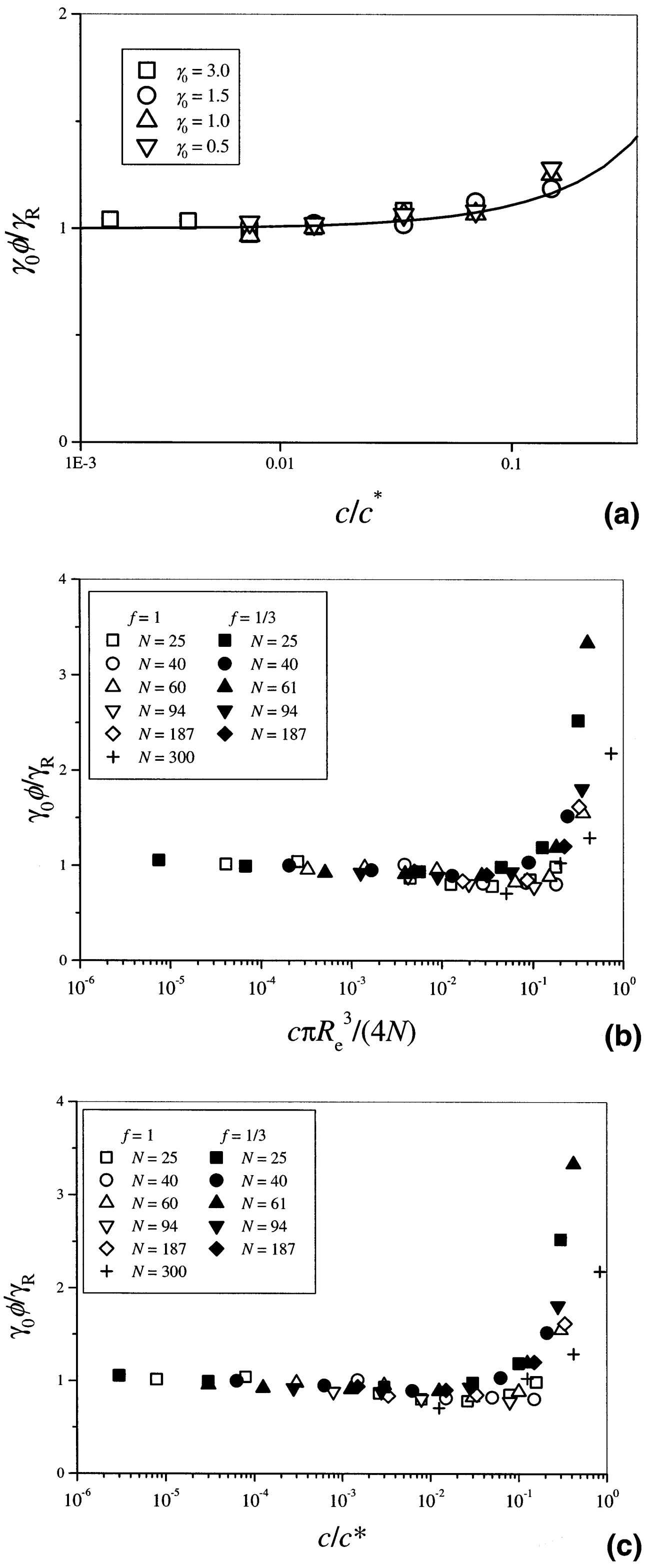

Figure 8. Universal plots of $\gamma_0\phi/\gamma_R$ vs normalized polymer concentration (a) rigid and (b, c) flexible chains. The solid line in (a) corresponds to eq 15.

The simple scaling theory[24,25] does not provide the expression for the fraction of counterions contributing to the osmotic pressure in semidilute solution. However, this can be done in the framework of Katchalsky's cell model.[20] In Katchalsky's cell model a semidilute polyelectrolyte solution is represented as a periodic array of chains separated by distance $R = [g_\xi/(\pi\xi c)]^{1/2}$, where ξ and g_ξ are the correlation length and number of monomers within the correlation length, respectively. The osmotic coefficient of Katchalsky's cell model is given by eq 11. To evaluate the osmotic coefficient, we have to know two parameters α and γ_0. The evaluation of the parameter γ_0 is straightforward, using the number of monomers g_ξ within the correlation length ξ. In the case of pure complex values of the parameter

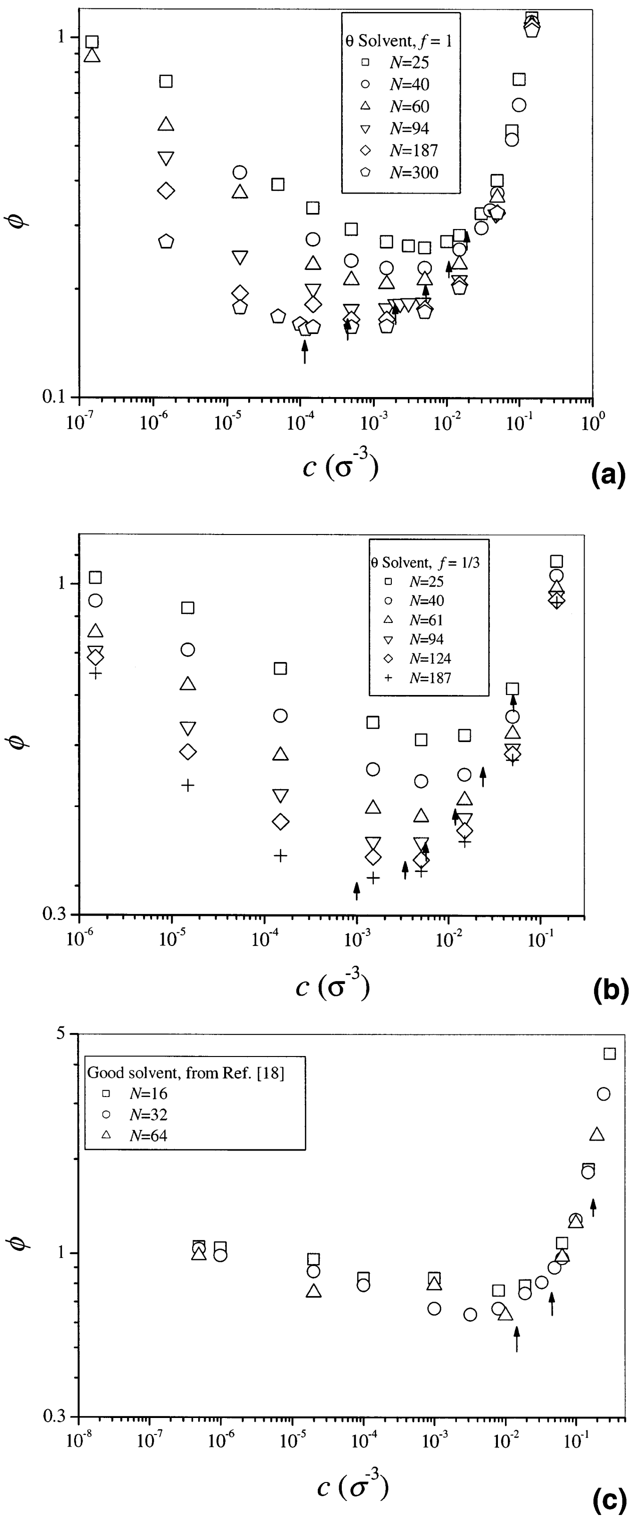

Figure 9. Dependence of the osmotic coefficient of flexible polyelectrolytes on polymer concentrations for fully (a) $f = 1$ and partially (b) $f = {}^1/_3$ charged chains in a Θ-solvent. Data from ref 18 for partially charged chains with $f = {}^1/_3$ in a good solvent (c). The arrows in (a), (b), and (c) show the overlap concentrations at various chain lengths N.

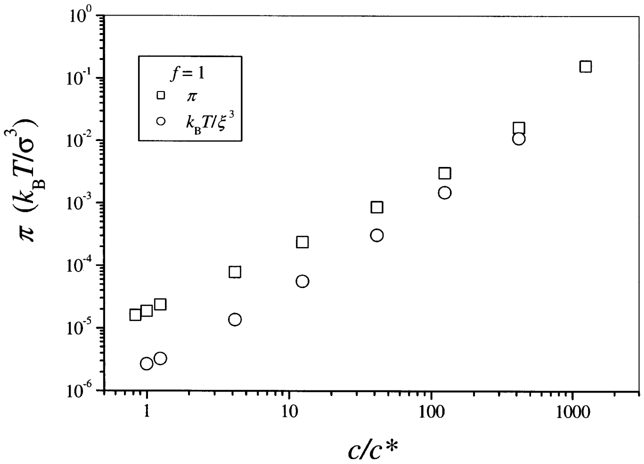

Figure 10. Comparison of the total osmotic pressure π in semidilute polyelectrolyte solution with polymeric contribution estimated as $k_B T/\xi^3$ for fully charged $f = 1$ flexible chains with $N = 300$.

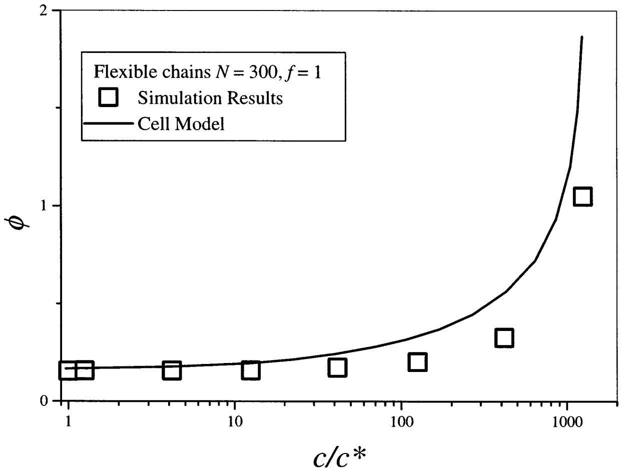

Figure 11. Comparison of the osmotic coefficient in semidilute polyelectrolyte solution with that estimated from Katchalsky's cell model (using eqs 11 and 18).

α, it satisfies the following nonlinear equation obtained from the boundary conditions (eq 6):

$$|\alpha| \ln\left(\frac{R}{\sigma}\right) = \arctan\left(\frac{1}{|\alpha|}\right) + \arctan\left(\frac{\gamma_0 - 1}{|\alpha|}\right) \qquad (18)$$

The results of the evaluation of the osmotic coefficient from Katchalsky's cell model[20] are shown in Figure 11. The predictions of the cell model agree reasonably well with our simulation results for $c < 100c^*$. Nevertheless, the cell model systematically overestimates the osmotic coefficient, and the largest deviations are observed in the concentration interval where polymeric contribution to the osmotic pressure becomes comparable to the one due to counterions.

Figure 12a shows the correlations between the overlap concentration c^* and the concentration $c_{\min}$ corresponding to the minimum of the osmotic coefficient of fully $f = 1$ and partially $f = {}^1/_3$ charged flexible chains at various chain lengths. In our simulations we used B-splines[27] to fit the simulation data for the osmotic coefficient around the minimum to determine the position $c_{\min}$ and the minimum value of the osmotic coefficient $\phi_{\min}$. Our results indicate that for longer chains the position of the minimum of the osmotic coefficient $c_{\min}$ approaches the overlap concentration c^*. However, for shorter chains the minimum systematically falls below c^* toward the dilute regime. For our shortest chains with number of monomers $N = 25$, $c_{\min}$ is about 8 times smaller than the overlap concentration c^*. At this concentration the distance between chains is only twice larger than their size.

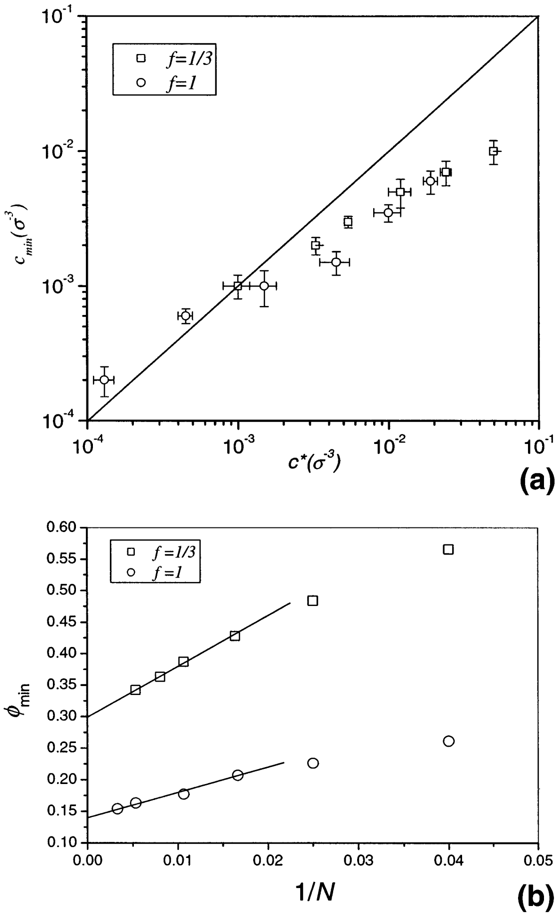

Figure 12. (a) Correlation between overlap concentration and position of the minimum of concentration dependence of the osmotic coefficient of flexible chain for fully ($f = 1$) and partially ($f = {}^1/_3$) charged chains (logarithmic scales). The solid line has slope 1.0. (b) Dependence of the minimum of osmotic coefficient on the chain degree of polymerization N. The intercepts are 0.14 and 0.3 for $f = 1$ and $f = {}^1/_3$, respectively.

The proportionality between $c_{\min}$ and overlap concentration c^* is in good qualitative agreement with the predictions of the two-zone model. According to the two-zone model, the osmotic coefficient is a decreasing function of polymer concentration in dilute solutions with nonzero values of the parameter γ_R.[14,15] However, in semidilute solutions ($\gamma_R = 0$), the osmotic coefficient increases with increasing the polymer concentration.[14,15,20,21] Thus, the crossover between increasing and decreasing behavior should occur around overlap concentration c^*.

Figure 12b shows the dependence of the minimum value of the osmotic coefficient $\phi_{\min}$ on the chain degree of polymerization N. This minimum value $\phi_{\min}$ is weakly dependent on the chain length and has asymptotic values of 0.14 for the fully ($f = 1$) and 0.30 for partially ($f = {}^1/_3$) charged chains. The limit of infinite N corresponds to infinite dilution limit ($R \rightarrow \infty$) for Katchalsky's cell model and to the overlap condition of "infinite" chains for the two-zone model. The value of the osmotic coefficient ϕ approaches the Manning limit $(2\gamma_0)^{-1}$ at infinite dilution in Katchalsky's cell model. Using the limiting values $\phi_{\min} = 0.14$ and $\phi_{\min} = 0.3$ for $N \to \infty$, we can evaluate the limiting values of the linear charge densities γ_0 for fully and partially charged FENE chains. These values are $\gamma_0 = 3.57$ ($f = 1$) and $\gamma_0 = 1.67$ ($f = {}^1/_3$). The obtained values of the parameter γ_0 are larger than that for rodlike chains with the same fraction of charged monomers ($\gamma_0 = 3$ for $f = 1$ and $\gamma_0 = 1$ for $f = {}^1/_3$), implying that flexible chains have higher linear charge density. This difference suggests that flexible chains with very large N could be not fully stretched at their overlap concentration.

6. Conclusion

We have presented a molecular dynamics study of the osmotic pressure and its relation to the counterion condensation in solutions of rodlike and flexible polyelectrolytes. To analyze our data, we used a two-zone model that describes not only semidilute but also dilute polyelectrolyte solutions.

Our simulation results for rigid chains are in excellent agreement with predictions of the two-zone model. We have been able to identify different phase regions depending on the values of linear charge densities on rigid polyion γ_0 and of the cylindrical region γ_R (see Figure 3).

The comparison of the counterion density profiles obtained in our simulations with analytical solution of the nonlinear Poisson−Boltzmann equation for the two-zone model clearly shows that this model is in good quantitative agreement with the simulation results in dilute solutions (see Figure 4). However, as polymer concentration approaches the overlap concentration, this agreement is not so good. It turns out that the analytical solution overestimates the electrostatic interactions, leading to higher counterion density in comparison with that obtained in simulations.

In dilute solutions the osmotic coefficient of rodlike chains decreases with increasing polymer concentration. This concentration dependence of the osmotic coefficient agrees well with the predictions of the two-zone model (see Figures 7a and 8a) and shows that osmotic coefficient in dilute solutions is proportional to the ratio of fractions of counterions γ_R/γ_0 distributed outside and inside the volume of a polyelectrolyte chain. This is in contrast with the classical result[20] that states the osmotic coefficient in a dilute solution is proportional to the fraction of free counterions $1/\gamma_0$. This discrepancy is not surprising since the classical result was obtained in the infinite dilution limit of Katchalsky's cell model that even in this limit keeps cylindrical cell electroneutral. The two-zone model eliminates the electroneutrality requirement for the cylindrical zone, providing correct asymptotic behavior in the dilute regime. The decrease of the osmotic coefficient in dilute solutions also agrees with the results that Gonzalez-Mozuelos and Olvera de la Cruz[28] obtained in the framework of three-dimensional cell model describing dilute solutions of charged objects with different fractal dimensionality. They have shown that the fraction of condensed counterions increases with increasing the polymer concentration.

Similar analysis of our simulation data was performed in dilute solutions of flexible polyelectrolytes. With increasing polymer concentration the fraction of counterions within the chain volume increases, leading to reduction of the net charge of the cylindrical region and the corresponding reduction of the chain size. Flexible chains contract with increasing polymer concentration,[18,20] and the bare linear charge density on them increases. Thus, for flexible chains the linear charge density γ_0 used in the two-zone model has to be reevaluated at each polymer concentration. Using this adjustment, we determined different regions in the phase diagram in the $\gamma_0-\gamma_R$ plane (see Figure 5).

The osmotic coefficient of flexible polyelectrolytes exhibits nonmonotonic dependence on polymer concentration. It decreases with polymer concentration in dilute solutions where it also follows the simplified expression eq 13 (see Figure 8b). Osmotic coefficient increases at higher concentrations. The upturn in the osmotic coefficient occurs around the overlap concentration c^*. Our simulation results show that for the longest chains ($N = 300$, 187, and 94) the position of the minimum of the osmotic coefficient $c_{\min}$ approaches the overlap concentration c^*, while for shortest ones it could be as much as an order of magnitude below c^* (see Figure 12a). The nonmonotonic behavior of the osmotic coefficient with polymer concentration is in good qualitative agreement with the predictions of the two-zone model. According to the two-zone model, the osmotic coefficient is a deceasing function of polymer concentration in dilute solutions whereas it is an increasing function of concentration in semidilute solutions. The crossover between these two regimes occurs around the overlap concentration c^*, where the spherical zone in the two-zone model disappears and the two-zone model reduces to the classical Katchalsky's cell model.

Unfortunately, we are not aware of experiments showing nonmonotonic dependence of the osmotic coefficient on polymer concentration. To see experimentally such nonmonotonic dependence of the osmotic coefficient, one has to satisfy the following conditions: The contribution of the counterions to the osmotic pressure should be larger than that of the residual salt. The lowest concentration of the residual salt accessible in experiments is of the order of 10^{-5} M. Since the minimum in the osmotic coefficient observed in our simulations is around overlap concentration, the overlap concentration c^* of a polyelectrolyte solution should be above 10^{-3} M for the salt contribution to the osmotic pressure to remain negligible. Thus, one can use, for example, fully sulfonated polystyrene with about 100−300 repeat units to see an experimentally nonmonotonic dependence of the osmotic coefficient on polymer concentration.

In semidilute polyelectrolyte solutions our simulations confirmed the fact that osmotic pressure is dominated by counterions in a wide concentration range (see Figure 10). Katchalsky's cell model (eq 11) provides a reasonable quantitative estimate for the osmotic coefficient (see Figure 11). The difference between the estimated value of the osmotic coefficient and the one obtained in our simulations does not exceed 20% over the wide range of polymer concentrations. The agreement becomes poor at higher polymer concentrations where the polymeric contribution to the osmotic pressure k_BT/ξ^3 is comparable to that due to counterions.

Acknowledgment. The authors are grateful to the National Science Foundation for the financial support under Grant DMR-0102267 and to the donors of the Petroleum Research Fund, administered by the American Chemical Society, for the financial support under Grant 37018-AC7.

References and Notes

(1) Kern, W. *Z. Phys Chem. (Munich)* **1938**, *A181*, 249; **1939**, *A184*, 197, 302.

(2) Auer, H. E.; Alexandrowicz, Z. *Biopolymers* **1969**, *8*, 1.

(3) Reddy, M.; Marinsky, J. A. *J. Phys. Chem.* **1970**, *74*, 3884.

(4) Takahashi, A.; Kato, N.; Nagasawa, M. *J. Phys. Chem.* **1970**, *74*, 944.

(5) Kozak, D.; Kristan, J.; Dolar, D. *Z. Phys. Chem. (Munich)* **1971**, *76*, 85.

(6) Oman, S. *Macromol. Chem.* **1974**, *175*, 2133.

(7) Oman, S. *Macromol. Chem.* **1977**, *178*, 475.

(8) Wang, L.; Bloomfield, V. A. *Macromolecules* **1990**, *23*, 804.

(9) Kakehashi, R.; Yamazoe, H.; Maeda, H. *Colloid Polym. Sci.* **1998**, *276*, 28.

(10) Manning, G. S. *J. Chem. Phys.* **1969**, *51*, 924. Oosawa, F. *Polyelectrolyte*; M. Dekker: New York, 1971.

(11) Fuoss, R. M.; Katchalsky, A.; Lifson, S. *Proc Natl. Acad. Sci. U.S.A.* **1951**, *37*, 579. Alfrey, T., Jr.; Berg, T. W.; Morawetz, H. *J. Polym. Sci.* **1951**, *7*, 543.

(12) Nilsson, L. G.; Guldbrand, L.; Nordenskiold, L. *Mol. Phys.* **1991**, *72*, 177. Das, T.; Bratko, D.; Bhuiyan, L. B.; Outhwaite, C. W. *J. Chem. Phys.* **1997**, *107*, 9197.

(13) Deserno, M.; Holm, C.; Kremer, K. *Macromolecules* **2000**, *33*, 199.

(14) Deshkovski, A.; Obukhov, S. P.; Rubinstein, M. *Phys. Rev. Lett.* **2001**, *86*, 2341.

(15) Deshkovski, A. Ph.D. Thesis, University of North Carolina at Chapel Hill, 2001.

(16) Blaul, J.; Wittemann, M.; Ballauff, M.; Rehahn, M. *J. Phys. Chem. B* **2000**, *104*, 7077.

(17) Raspaud, E.; de Conceicao, M.; Livolant, F. *Phys. Rev. Lett.* **2000**, *84*, 2533.

(18) Stevens, M.; Kremer, K. *J. Chem. Phys.* **1995**, *103*, 1669.

(19) Liao, Q.; Dobrynin, A. V.; Rubinstein, M. *Macromolecules* **2003**, *36*, 3386.

(20) Katchalsky, A.; Alexandrowicz, Z.; Keden, O. In *Chemical Physics of Ionic Solutions*; Conway, B. E., Barradas, R. O., Eds.; Wiley: New York, 1966; p 266.

(21) Beloni, L.; Drifford, M.; Turq, P. *Chem. Phys.* **1984**, *83*, 147.

(22) Essman, U.; Perera, L.; Berkovitz, M. L. *J. Chem. Phys.* **1995**, *103*, 8577.

(23) Allen, M. P.; Tildesley, D. J. *Computer Simulation of Liquids*; Clarendon Press: Oxford, 1987.

(24) deGennes, P.-G.; Pincus, P.; Velasco, R. M.; Brochard, F. *J. Phys.* (*Paris*) **1976**, *37*, 1461.

(25) Dobrynin, A. V.; Colby, R. H.; Rubinstein, M. *Macromolecules* **1995**, *28*, 1859.

(26) deGennes, P.-G. *Scaling Concepts in Polymer Physics;* Cornell University Press: Ithaca, NY, 1979.

(27) Chui, C. K. *An Introduction to Wavelets;* Academic Press: San Diego, CA, 1992.

(28) Gonzalez-Mozuelos, P.; Olvera de la Cruz, M. *J. Chem. Phys.* **1995**, *103*, 3145.

MA0259968